

Movable Antenna-Enabled Co-Frequency Co-Time Full-Duplex Wireless Communication

Jingze Ding, *Graduate Student Member, IEEE*, Zijian Zhou, *Member, IEEE*, Wenyao Li, Chenbo Wang, *Graduate Student Member, IEEE*, Lifeng Lin, and Bingli Jiao, *Senior Member, IEEE*

Abstract—Movable antenna (MA) provides an innovative way to arrange antennas that can contribute to improved signal quality and more effective interference management. This method is especially beneficial for co-frequency co-time full-duplex (CCFD) wireless communication, which struggles with self-interference (SI) that usually overpowers the desired incoming signals. By dynamically repositioning transmit/receive antennas, we can mitigate the SI and enhance the reception of incoming signals. Thus, this paper proposes a novel MA-enabled point-to-point CCFD system and formulates the minimum achievable rate of two CCFD terminals. To maximize the minimum achievable rate and determine the near-optimal positions of the MAs, we introduce a solution based on projected particle swarm optimization (PPSO), which can circumvent common suboptimal positioning issues. Moreover, numerical results reveal that the PPSO method leads to a better performance compared to the conventional alternating position optimization (APO). The results also demonstrate that an MA-enabled CCFD system outperforms the one using fixed-position antennas (FPAs).

Index Terms—Movable antenna (MA), co-frequency co-time full-duplex (CCFD), fixed-position antenna (FPA), projected particle swarm optimization (PPSO).

I. INTRODUCTION

WIRELESS communications are experiencing a dramatic increase in the demand for never-enough capacity and thus, the spectrum resources become ever more precious towards the sixth generation (6G). To rise to this challenge, co-frequency co-time full-duplex (CCFD) wireless communication [1], [2] stands out as a potential for doubling spectral efficiency by enabling the simultaneous exchange of information across the same frequency band. However, the presence of self-interference (SI) that is leaked from the transmitter's antenna poses a troublesome impediment to practical applications of this technology.

In the field of antennas, the SI can be mitigated to a certain extent through passive methods, such as separate distance, orientation, and polarization [3]–[5], whilst active analog and digital cancellation techniques have been extensively studied. For better SI cancellation, researchers have delved into the realm of antenna design, exploring how it can play a more dynamic role. This pursuit leads to the development of the

antenna selection (AS) method [6], a technique designed to exploit the potential of spatial degrees of freedom (DoFs). In [7], the authors investigate the impact of increasing the number of AS elements and observe that, although such an increase can improve the system performance, it also raises the cost of implementation due to the requisite rise in radio frequency channels. Furthermore, placing AS elements in close proximity risks antenna coupling, which could lead to reduced antenna efficiency.

Considering the limitations of AS, the authors in [8]–[11] first describe the concept of fluid antenna system (FAS), which takes advantage of liquid-based antennas with flexible antenna architectures. Specifically, they explore the use of a single antenna that can be moved to various preset locations along a linear axis. This approach has shown that the FAS can reduce interference and enhance the signal of interest (SoI) far better than traditional systems that rely on a limited array of antennas to perform maximum ratio combining. Further advancements are presented by the authors in [12], where the FAS is expanded into a system aided by movable antennas (MAs). These antennas can be precisely positioned using stepper motors, allowing for movement in a three-dimensional space, which could significantly improve signal reception. The study [7] provides the modeling and performance analysis of these MA-enabled wireless communication systems, considering various channel models to give a comprehensive understanding of their capabilities. In multiple-input multiple-output (MIMO) systems, the study [13] investigates how the MA technology can be utilized. It shows that by alternatively optimizing the transmit covariance matrix and the position of each MA while keeping other variables fixed, the system's data rate can be significantly increased. The challenge of multiuser uplink communication is addressed in [14], [15]. These studies explore strategies for multiple single-antenna users who communicate with a base station equipped with an MA array, aiming to minimize overall transmission power while maximizing the minimum achievable rate of all users, thereby ensuring a robust connection.

The advantages of the MA technology can be summarized as its capability to dynamically leverage spatial DoFs through the superposition of transmit/receive signals across various wireless channels [7], [12]–[15]. This characteristic is crucial in reducing interference and enhancing the SoI, making the MA especially well-suited for CCFD wireless applications. To the best of our knowledge, this technology has not yet been considered in CCFD wireless systems. Motivated by these considerations, we propose a novel point-to-point CCFD system

This work was jointly supported by the Science and Technology Project of Guangzhou under Grants 202206010118 and 2023B04J0011. The calculations were supported by the High-Performance Computing Platform of Peking University. (*Corresponding author: Zijian Zhou.*)

J. Ding, Z. Zhou, W. Li, C. Wang, L. Lin, and B. Jiao are with the Department of Electronics, Peking University, Beijing 100871, China (e-mail: djz@stu.pku.edu.cn; zjzhou1008@pku.edu.cn; liwenyao@stu.pku.edu.cn; {wcb15, linlifeng, jiaobl}@pku.edu.cn).

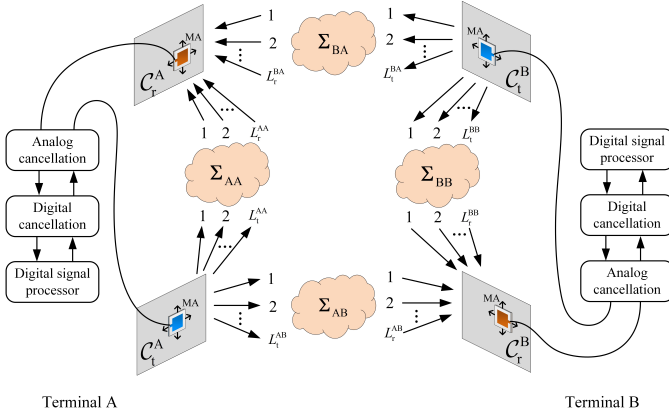


Fig. 1. An MA-enabled point-to-point CCFD wireless system

assisted by the MAs. In particular, our main contributions to this work are threefold. First, we formulate the optimization problem by maximizing the minimum achievable rate of two CCFD terminals with the aid of the MAs. Next, to circumvent an undesired sub-optimal positioning, we introduce projected particle swarm optimization (PPSO) as a superior alternative to the conventional alternating position optimization (APO) approach. Last, we provide simulation results that not only illustrate a better performance of the PPSO method over traditional solutions but also substantiate the enhancements of an MA-enabled CCFD system compared to systems with fixed-position antennas (FPAs).

Notation: a , \mathbf{a} , and \mathbf{A} denote a scalar, a vector, and a matrix, respectively. $(\cdot)^T$ and $(\cdot)^H$ stand for transpose and conjugate transpose, respectively. Besides, \odot represents Hadamard product. We use $[\mathbf{a}]_i$ to denote the i^{th} element of the vector \mathbf{a} . The circularly symmetric complex Gaussian (CSCG) distribution with mean zero and variance σ^2 is represented by $\mathcal{CN}(0, \sigma^2)$.

II. SYSTEM MODEL

Figure 1 depicts an MA-enabled point-to-point CCFD wireless system that comprises terminals A and B. Each terminal is equipped with a single transmit antenna and a single receive antenna. These antennas can be facilitated by stepper motors, allowing them to move within a two-dimensional region. The transmit and receive positions of the MAs are denoted using Cartesian coordinates, i.e., $\mathbf{t}_p = [x_t^p, y_t^p]^T \in \mathcal{C}_t^p$ and $\mathbf{r}_q = [x_r^q, y_r^q]^T \in \mathcal{C}_r^q$, where \mathcal{C}_t^p and \mathcal{C}_r^q are the respective transmit and receive regions at terminals p and q . Herein, p and q belong to the set $\{A, B\}$, signifying the terminal labels. This notation will be consistently used in the following derivations.

In this MA-enabled CCFD wireless system, the channel response relies on the variable positions of the MAs. We thus characterize the channel coefficient as a function of the transmit and receive MAs' coordinates, i.e., $h_{pq}(\mathbf{t}_p, \mathbf{r}_q)$. Assuming the transmit power of the terminals is denoted by P_t , the received signals at terminal q can be expressed as

$$z_q(\mathbf{t}_p, \mathbf{r}_q) = h_{pq}(\mathbf{t}_p, \mathbf{r}_q) \sqrt{P_t} s_p + h_{qq}(\mathbf{t}_q, \mathbf{r}_q) \sqrt{P_t} s_q + n_q, \quad p \neq q. \quad (1)$$

Here, s_p and s_q stand for transmitted signals with zero mean and normalized power of one. $n_q \sim \mathcal{CN}(0, \sigma_q^2)$ is the additive white Gaussian noise (AWGN) with power of σ_q^2 . Besides, the first term in (1) represents the SoI, while the second term is the inherent SI in CCFD systems.

It is worth noting that the positions of the MAs don't directly influence the performance of the analog and digital cancellations, as they are capable of actively mitigating the SI by adapting to channel variations. Considering this, we will focus on exploring the potential of cancellation in the antenna domain.

A. Channel Model

Referring to the channel modeling in [7], we define the positions of the FPAs by setting $\mathbf{t}_p = [0, 0]^T$ and $\mathbf{r}_q = [0, 0]^T$. Then, the channel matrix from the transmit MA of terminal p to the receive MA of terminal q can be given by Σ_{pq} of dimension $L_r^{pq} \times L_t^{pq}$, where L_t^{pq} and L_r^{pq} represent the number of transmit and receive paths, respectively. Compared to the FPAs, the difference of propagation distance for the MAs at the l^{th} transmit path can be expressed as

$$\rho_{t,l_t}^p(\mathbf{t}_p) = x_t^p \cos \theta_{t,l_t}^p \sin \phi_{t,l_t}^p + y_t^p \sin \theta_{t,l_t}^p, \quad l_t = 1, 2, \dots, L_t^{pq}. \quad (2)$$

Similarly,

$$\rho_{r,l_r}^q(\mathbf{r}_q) = x_r^q \cos \theta_{r,l_r}^q \sin \phi_{r,l_r}^q + y_r^q \sin \theta_{r,l_r}^q, \quad l_r = 1, 2, \dots, L_r^{pq} \quad (3)$$

represents the difference at the l_r^{th} receive path.

In (2) and (3), θ_{t,l_t}^p and ϕ_{t,l_t}^p respectively denote the elevation and azimuth angles of departure (AoDs) at the l_t^{th} transmit path, while θ_{r,l_r}^q and ϕ_{r,l_r}^q respectively denote the elevation and azimuth angles of arrival (AoAs) at the l_r^{th} receive path. Here, $-\frac{\pi}{2} \leq \theta_{t,l_t}^p, \phi_{t,l_t}^p, \theta_{r,l_r}^q, \phi_{r,l_r}^q \leq \frac{\pi}{2}$. The phase difference between the antennas can be written by $\frac{2\pi\rho}{\lambda}$, where ρ is the difference of propagation distance and λ is the wavelength. Then, the field-response vectors are respectively given by

$$\mathbf{g}(\mathbf{t}_p) = \left[e^{j\frac{2\pi}{\lambda}\rho_{t,1}^p(\mathbf{t}_p)}, e^{j\frac{2\pi}{\lambda}\rho_{t,2}^p(\mathbf{t}_p)}, \dots, e^{j\frac{2\pi}{\lambda}\rho_{t,L_t^{pq}}^p(\mathbf{t}_p)} \right]^T \quad (4)$$

and

$$\mathbf{f}(\mathbf{r}_q) = \left[e^{j\frac{2\pi}{\lambda}\rho_{r,1}^q(\mathbf{r}_q)}, e^{j\frac{2\pi}{\lambda}\rho_{r,2}^q(\mathbf{r}_q)}, \dots, e^{j\frac{2\pi}{\lambda}\rho_{r,L_r^{pq}}^q(\mathbf{r}_q)} \right]^T. \quad (5)$$

As a result, the channel coefficient between the transmit and receive MAs can be obtained by

$$h_{pq}(\mathbf{t}_p, \mathbf{r}_q) = \mathbf{f}(\mathbf{r}_q)^H \Sigma_{pq} \mathbf{g}(\mathbf{t}_p). \quad (6)$$

B. Problem Formulation

For CCFD wireless communication, the signal-to-interference-plus-noise ratio (SINR) is an important metric to evaluate the system performance. In this scenario, it can be represented by

$$\gamma^q = \frac{|h_{pq}(\mathbf{t}_p, \mathbf{r}_q)|^2 P_t}{|h_{qq}(\mathbf{t}_q, \mathbf{r}_q)|^2 P_t + \sigma_q^2}, \quad p \neq q. \quad (7)$$

Therefore, based on (7), the achievable rate at terminal q is calculated by

$$R_q = \log_2(1 + \gamma^q). \quad (8)$$

For the purpose of ensuring fairness between the terminals, we aim to maximize the minimum achievable rate by jointly optimizing the positions of the four MAs. To this end, the optimization problem is formulated as

$$\max_{\mathbf{t}_p, \mathbf{r}_q} \min\{R_A, R_B\} \quad (9)$$

$$\text{s.t. } \mathbf{t}_p \in \mathcal{C}_t^p, \quad (9a)$$

$$\mathbf{r}_q \in \mathcal{C}_r^q, \quad (9b)$$

$$p, q \in \{A, B\}. \quad (9c)$$

Constraints (9a) and (9b) indicate that the MAs are confined to movement within a determined transmit/receive region. Even though problem (9) appears simple, it is difficult to solve in virtue of the non-convex objective function. Moreover, the position of each transmit/receive MA has a significant impact not only on the reception of the SoI but also on the SI, thereby leading to a relatively strong interrelationship among the positions of all four MAs.

III. PROPOSED SOLUTION

Due to the non-convex nature of the objective function in problem (9), the conventional APO method, which involves alternately fixing three MAs while moving only one, risks converging to an undesired local optimum. Besides, traversal algorithms to identify the optimal solution require exploring an extensive space, resulting in prohibitively high computational complexity. Taking these factors into account, this section investigates the PPSO method [14], which supports the simultaneous optimization of all four MAs' positions.

A. PPSO Method

To begin with, denoting N as the total number of particles and K as the number of iterations, the positions of the MAs during the k^{th} iteration are represented by a position matrix, i.e., $\mathbf{U}^{(k)} = [\mathbf{u}_1^{(k)}, \mathbf{u}_2^{(k)}, \dots, \mathbf{u}_n^{(k)}, \dots, \mathbf{u}_N^{(k)}]$ of dimension $8 \times N$, where $k = 0, 1, \dots, K$ and $n = 1, 2, \dots, N$. The position vector of the n^{th} particle is defined as

$$\mathbf{u}_n^{(k)} = \left[\mathbf{t}_{A,n}^{(k)T}, \mathbf{r}_{A,n}^{(k)T}, \mathbf{t}_{B,n}^{(k)T}, \mathbf{r}_{B,n}^{(k)T} \right]^T, \quad (10)$$

where $\mathbf{t}_{p,n}^{(k)}$ and $\mathbf{r}_{q,n}^{(k)}$ represent the transmit and receive MAs' coordinates of the terminals, respectively, and $\mathbf{u}_n^{(k)}$ might be a potential solution to problem (9). The velocity matrix for the particles is introduced as $\mathbf{V}^{(k)} = [\mathbf{v}_1^{(k)}, \mathbf{v}_2^{(k)}, \dots, \mathbf{v}_n^{(k)}, \dots, \mathbf{v}_N^{(k)}]$ of dimension $8 \times N$.

For constraints (9a) and (9b), the coordinates $\mathbf{t}_{p,n}^{(k)}$ and $\mathbf{r}_{q,n}^{(k)}$ in (10) are restricted to given regions. We assume \mathcal{C}_t^p and \mathcal{C}_r^q are square regions, each with size $D \times D$. Therefore, the vector $\mathbf{u}_n^{(k)}$ is updated as

$$\mathbf{u}_n^{(k)} = \mathcal{D} \left\{ \mathbf{u}_n^{(k-1)} + \mathbf{v}_n^{(k)} \right\}, \quad k = 1, 2, \dots, K. \quad (11)$$

Algorithm 1 PPSO method

Input: $\{\mathcal{C}_t^p\}, \{\mathcal{C}_r^q\}, \{\theta_{t,t}^p\}, \{\phi_{t,t}^p\}, \{\theta_{r,t}^q\}, \{\phi_{r,t}^q\}, N, K, c_1, c_2, \mathbf{e}_1, \mathbf{e}_2, \omega_{\min}, \omega_{\max}$.

Output: \mathbf{u}^* .

- 1: Randomly initialize the position matrix $\mathbf{U}^{(0)}$ and the velocity matrix $\mathbf{V}^{(0)}$.
 - 2: Initialize the local and global optimum position vectors, \mathbf{u}_n^* and \mathbf{u}^* , respectively.
 - 3: **for** $k = 1$ to K **do**
 - 4: Calculate the inertia weight ω .
 - 5: **for** $n = 1$ to N **do**
 - 6: Calculate the position and velocity vectors of the n^{th} particle, $\mathbf{u}_n^{(k)}$ and $\mathbf{v}_n^{(k)}$, respectively.
 - 7: Update the fitness value of the n^{th} particle $F(\mathbf{u}_n^{(k)})$.
 - 8: **if** $F(\mathbf{u}_n^{(k)}) > F(\mathbf{u}_n^*)$ **then**
 - 9: $\mathbf{u}_n^* = \mathbf{u}_n^{(k)}$.
 - 10: **end if**
 - 11: **if** $F(\mathbf{u}_n^{(k)}) > F(\mathbf{u}^*)$ **then**
 - 12: $\mathbf{u}^* = \mathbf{u}_n^{(k)}$.
 - 13: **end if**
 - 14: **end for**
 - 15: **end for**
 - 16: **return** \mathbf{u}^* .
-

$\mathcal{D}(\mathbf{a})$ specifies a function that projects each component of vector \mathbf{a} to its corresponding maximum/minimum value, i.e.,

$$[\mathcal{D}\{\mathbf{a}\}]_i = \begin{cases} \frac{D}{2}, & \text{if } [\mathbf{a}]_i > \frac{D}{2} \\ [\mathbf{a}]_i, & \text{if } -\frac{D}{2} \leq [\mathbf{a}]_i \leq \frac{D}{2} \\ -\frac{D}{2}, & \text{if } [\mathbf{a}]_i < -\frac{D}{2} \end{cases}. \quad (12)$$

In the PPSO method, incorporating with (11), the velocity vector for the n^{th} particle at the k^{th} iteration is calculated by

$$\mathbf{v}_n^{(k)} = \omega \mathbf{v}_n^{(k-1)} + c_1 \mathbf{e}_1 \odot (\mathbf{u}_n^* - \mathbf{u}_n^{(k-1)}) + c_2 \mathbf{e}_2 \odot (\mathbf{u}^* - \mathbf{u}_n^{(k-1)}), \quad k = 1, 2, \dots, K. \quad (13)$$

Here, the inertia weight, ω , is pivotal in moderating the impact of the prior velocity, $\mathbf{v}_n^{(k-1)}$, on the subsequent velocity, $\mathbf{v}_n^{(k)}$. The learning factors, c_1 and c_2 , serve as step sizes that guide each particle towards the local optimum position vector, \mathbf{u}_n^* , and the global optimum position vector, \mathbf{u}^* . Furthermore, the random vectors, \mathbf{e}_1 and \mathbf{e}_2 , filled with 8 elements that are typically uniform random numbers within the range $[0, 1]$, are used to increase the randomness of the search for the sake of reducing the risk of settling on an unfavorable local optimum.

To balance the trade-off between the speed and precision of the PPSO search, ω is described as a linearly decreasing function across the iteration count in the interval $[\omega_{\min}, \omega_{\max}]$, calculated as $\omega = \omega_{\max} - (\omega_{\max} - \omega_{\min}) \frac{k}{K}$. During each iteration, the fitness function determines the local and global optimum position vectors, assuming the premise that the best position vector corresponds to the largest fitness value. To

TABLE I
SIMULATION PARAMETERS

| Parameter | Description | Value |
|--------------------------|--------------------------------------------|---------|
| α | Path loss exponent | 2.8 |
| β_{AA}, β_{BB} | Path loss coefficients of the SI | -90 dB |
| β_{AB}, β_{BA} | Path loss coefficients of the SoI | -30 dB |
| d_{AA}, d_{BB} | Propagation distances for the SI channels | 1 m |
| d_{AB}, d_{BA} | Propagation distances for the SoI channels | 100 m |
| σ_A^2, σ_B^2 | AWGN powers | -80 dBm |
| P_t | Transmit power | 20 dBm |
| N | Number of particles | 200 |
| K | Number of iterations | 100 |
| c_1, c_2 | Learning factors | 1.4 |
| ω_{\min} | Minimum inertia weight | 0.4 |
| ω_{\max} | Maximum inertia weight | 0.9 |

maximize the minimum achievable rate in (9), the fitness function of each particle is established as

$$F(\mathbf{u}_n^{(k)}) = \min \left\{ R_A(\mathbf{u}_n^{(k)}), R_B(\mathbf{u}_n^{(k)}) \right\}, \quad (14)$$

where $R_A(\mathbf{u}_n^{(k)})$ and $R_B(\mathbf{u}_n^{(k)})$ denote the achievable rates of the terminals when the positions of the MAs are specified by $\mathbf{u}_n^{(k)}$.

The PPSO method to address problem (9) is presented in Algorithm 1. Initially, in line 1, the particles are set up with the starting positions $\mathbf{U}^{(0)}$ and initial velocities $\mathbf{V}^{(0)}$. Following this, in line 2, the local optimum position vector for each particle is initialized by

$$\mathbf{u}_n^* = \mathbf{u}_n^{(0)}, \quad (15)$$

while the global optimum position vector is identified through

$$\mathbf{u}^* = \arg \max_{\mathbf{u}_n^{(0)}} \left[F(\mathbf{u}_1^{(0)}), F(\mathbf{u}_2^{(0)}), \dots, F(\mathbf{u}_N^{(0)}) \right]. \quad (16)$$

After these initializations, the algorithm progresses to the iterative phase (line 3). For each k^{th} iteration, the first step involves calculating the inertia weight ω (line 4), which is followed by the computation of both position and velocity vectors for each particle (line 6). The fitness value for every particle is updated according to (14) in line 7. Particularly noteworthy is the process from lines 8 to 13, where local and global optimum position vectors are updated in response to larger fitness values. Upon completing K iterations, the procedure yields the near-optimal positions of all four MAs, denoted as \mathbf{u}^* , in line 16.

B. Convergence and Complexity Analysis

The convergence of the PPSO method is ensured for two key reasons. Firstly, the global optimum position's fitness value either remains constant or increases over iterations since a position is only designated as the global optimum if it has a superior fitness value. Secondly, the minimum achievable rate for problem (9) is capped by an upper limit, which prevents indefinite increase. As for the computational complexity, the PPSO method operates with a complexity of $\mathcal{O}(NK)$, which is influenced by the total number of the particles, N , and the iterative times, K .

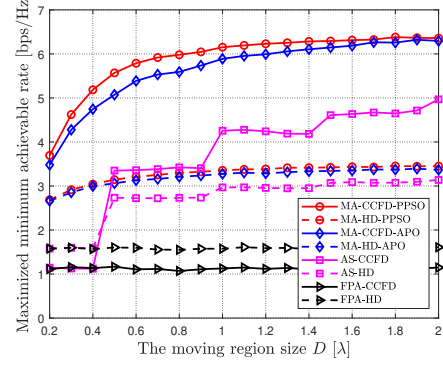


Fig. 2. Maximized minimum achievable rates vs. the moving region size D .

IV. SIMULATION RESULTS

In this section, we successively outline the simulation setup and provide performance comparisons. Numerical simulation results illustrate the performance of our proposed MA-enabled CCFD wireless system and imply the effectiveness of the PPSO method in maximizing the minimum achievable rate between the CCFD terminals.

For the simulation setup, we adopt the geometry channel model as [13], [14], in which the channel matrix Σ_{pq} is composed of L_{pq} diagonal elements that follow a CSCG distribution $\mathcal{CN}\left(0, \frac{\beta_{pq} d_{pq}^{-\alpha}}{L_{pq}}\right)$. Here, $L_t^{pq} = L_r^{pq} \triangleq L_{pq}$, α is the path loss exponent, β_{pq} represents the path loss coefficient, and d_{pq} denotes the propagation distance. Notably, when $p = q$, the matrix Σ_{pq} can be interpreted as the SI channel; for $p \neq q$, it indicates the SoI channel. It is important to emphasize that the path loss of the SI is considered to be much larger than that of the SoI, owing to the directionality of antennas and the assistance provided by both analog and digital cancellations. Thus, we assume $\beta_{pq} = -90$ dB with $p = q$ and $\beta_{pq} = -30$ dB with $p \neq q$ [16]. The elevation and azimuth AoDs and AoAs are assumed to be the independent and identically distributed (i.i.d.) random variables within the interval $[-\frac{\pi}{2}, \frac{\pi}{2}]$. Specifically, the detailed simulation parameters are listed in Table I.

We compare the performance of various schemes, including MA, FPA, and AS, as well as CCFD and half-duplex (HD) modes. We note that the rate in (8) is divided by two in the HD mode. Also, we evaluate the performance of our proposed algorithm (see Algorithm 1), against the conventional APO method. In the APO method, the moving region is partitioned into multiple grids of size $\frac{\lambda}{100} \times \frac{\lambda}{100}$, allowing for an alternative search of each MA's position while others remain fixed. In the AS-enabled scheme, the antenna arrays are deployed at intervals of $\frac{\lambda}{2}$ and optimal antennas are selected through alternating optimization. The antennas used in the aforementioned schemes cannot exceed the region of size $D \times D$. For convenience, our proposed scheme is referred to as MA-CCFD-PPSO, signifying the MA-enabled CCFD scheme that utilizes the PPSO method. Other schemes are labeled in a similar manner for straightforward comparison.

As shown in Fig. 2, we investigate the maximized minimum achievable rate concerning the moving region size D , consid-

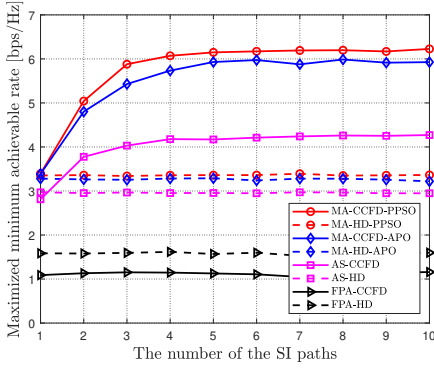


Fig. 3. Maximized minimum achievable rates vs. the number of the SI paths.

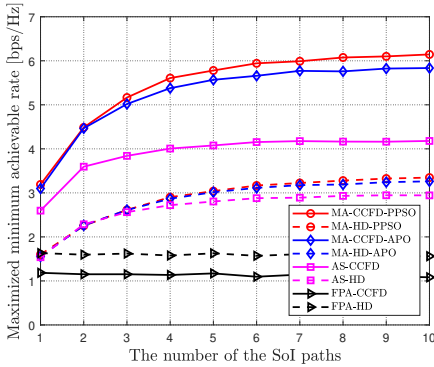


Fig. 4. Maximized minimum achievable rates vs. the number of the SoI paths.

ering $L_{pq} = 5$ for $p = q$ and $L_{pq} = 10$ for $q \neq p$. This figure reveals that for MA-enabled schemes, the rates continuously rise as the moving region expands. In contrast, in AS-enabled schemes, the increases in the rates are only noticeable when the number of deployed antennas is augmented and such an augmentation occurs if the size D is an integer multiple of $\frac{\lambda}{2}$. Compared to FPA-aided schemes, these schemes demonstrate enhanced performance. The PPSO method surpasses the APO method in performance, especially when the size D is smaller than λ in the CCFD mode. However, for the HD mode, the distinction in improvement is less pronounced, indicating that the PPSO method brings greater enhancements in scenarios of higher complexity. It is interesting to observe that the AS-enabled HD scheme exhibits superior performance over the CCFD one when the size $D < \frac{\lambda}{2}$. This superiority can be attributed to the deployment of a single antenna at the origin coordinate of the moving region, aligning its performance with that of the FPA-aided schemes. Owing to the presence of the SI, the CCFD mode underperforms in comparison to the HD mode, similar to the outcomes of the FPA-aided schemes.

Figure 3 depicts the maximized minimum achievable rates versus the number of the SI paths, given the number of the SoI paths $L_{pq} = 10$ with $p \neq q$ and $D = \lambda$. Correspondingly, Figure 4 shows the rates regarding the number of the SoI paths, where the number of the SI paths $L_{pq} = 5$ with $p = q$ and $D = \lambda$. In the CCFD mode, it can be seen that the rates for both MA-enabled and AS-enabled schemes increase with an increase in the number of the SI or SoI paths. However, in the

HD mode, the rates hold steady when the number of the SoI paths is constant, due to the absence of the SI. These results also imply that the PPSO method consistently outperforms the conventional APO method across different settings. Furthermore, all the discussed schemes present superior performance over the FPA-aided schemes.

V. CONCLUSION

In this paper, we propose a point-to-point CCFD system enhanced with the MAs. By dynamically repositioning antennas to simultaneously mitigate the SI and bolster the SoI, the MA-enabled CCFD system is capable of achieving an outstanding maximized minimum achievable rate. To effectively optimize the positions of the MAs, the PPSO method is implemented, addressing the non-convex problem and preventing convergence to an undesired suboptimal solution. Simulation results confirm the performance improvements offered by the PPSO method compared to the conventional APO method. Furthermore, these results highlight the superiority of the MA-enabled CCFD scheme over the AS-enabled schemes and those deploying FPAs regardless of whether they operate in the CCFD or HD modes.

REFERENCES

- [1] A. Sabharwal, P. Schniter, D. Guo, D. W. Bliss, S. Rangarajan, and R. Wichman, "In-band full-duplex wireless: challenges and opportunities," *IEEE J. Sel. Areas Commun.*, vol. 32, no. 9, pp. 1637-1652, Sep. 2014.
- [2] M. Ma, S. Tian, Y. Chen, L. Wang, Y. Yang, L. Wan, B. Jiao, and H. V. Poor, "A prototype of co-frequency co-time full duplex networking," *IEEE Wireless Commun.*, vol. 27, no. 1, pp. 132-139, Feb. 2020.
- [3] M. Duarte, C. Dick, and A. Sabharwal, "Experiment-driven characterization of full-duplex wireless systems," *IEEE Trans. Wireless Commun.*, vol. 11, no. 12, pp. 4296-4307, Dec. 2012.
- [4] M. Duarte and A. Sabharwal, "Full-duplex wireless communications using off-the-shelf radios: Feasibility and first results," in *Proc. Conf. Rec. 44th Asilomar Conf. Signals, Syst. Comput.*, Nov. 2010, pp. 1558-1562.
- [5] J. C. Dash and D. Sarkar, "A colinearly polarized full-duplex antenna with extremely high Tx-Rx isolation," *IEEE Antennas Wireless Propag. Lett.*, vol. 21, no. 12, pp. 2387-2391, Dec. 2022.
- [6] S. Sanayei and A. Nosratinia, "Antenna selection in MIMO systems," *IEEE Commun. Mag.*, vol. 42, no. 10, pp. 68-73, Oct. 2004.
- [7] L. Zhu, W. Ma, and R. Zhang, "Modeling and performance analysis for movable antenna enabled wireless communications," *IEEE Trans. Wireless Commun.*, Nov. 14, 2023, early access, DOI: 10.1109/TWC.2023.3330887.
- [8] K. -K. Wong, A. Shojaeifard, K. -F. Tong, and Y. Zhang, "Fluid antenna systems," *IEEE Trans. Wireless Commun.*, vol. 20, no. 3, pp. 1950-1962, Mar. 2021.
- [9] K. -K. Wong, W. K. New, X. Hao, K. -F. Tong, and C. -B. Chae, "Fluid antenna system—Part I: Preliminaries," *IEEE Commun. Lett.*, vol. 27, no. 8, pp. 1919-1923, Aug. 2023.
- [10] K. -K. Wong, K. -F. Tong, and C. -B. Chae, "Fluid antenna system—Part II: Research opportunities," *IEEE Commun. Lett.*, vol. 27, no. 8, pp. 1924-1928, Aug. 2023.
- [11] K. -K. Wong, K. -F. Tong, and C. -B. Chae, "Fluid antenna system—Part III: A new paradigm of distributed artificial scattering surfaces for massive connectivity," *IEEE Commun. Lett.*, vol. 27, no. 8, pp. 1929-1933, Aug. 2023.
- [12] L. Zhu, W. Ma, and R. Zhang, "Movable antennas for wireless communication: opportunities and challenges," *IEEE Commun. Mag.*, Oct. 16, 2023, early access, DOI: 10.1109/MCOM.001.2300212.
- [13] W. Ma, L. Zhu, and R. Zhang, "MIMO capacity characterization for movable antenna systems," *IEEE Trans. Wireless Commun.*, Sep. 7, 2023, early access, DOI: 10.1109/TWC.2023.3307696.
- [14] Z. Xiao, X. Pi, L. Zhu, X. Xia, and R. Zhang, "Multiuser communications with movable-antenna base station: joint antenna positioning, receive combining, and power control," *arXiv preprint arXiv:2308.09512*, 2023.

- [15] G. Hu, Q. Wu, K. Xu, J. Ouyang, J. Si, Y. Cai, and N. Al-Dhahir, "Movable-antenna array enabled multiuser uplink: a low-complexity gradient descent for total transmit power minimization," *arXiv preprint arXiv:2312.05763*, 2023.
- [16] P. Guan, Y. Wang, H. Yu, and Y. Zhao, "Joint beamforming optimization for RIS-aided full-duplex communication," *IEEE Wireless Commun. Lett.*, vol. 11, no. 8, pp. 1629-1633, Aug. 2022.